Acta Biomaterialia 7 (2011) 1150–1159

Contents lists available at ScienceDirect

Acta Biomaterialia

journal homepage: www.elsevier.com/locate/actabiomat

Polarized Raman analysis of the molecular rearrangement and residual strain on the surface of retrieved polyethylene tibial plates

Leonardo Puppulin [a], Yasuhito Takahashi [a], Wenliang Zhu [a], Nobuhiko Sugano [b], Giuseppe Pezzotti [a,*]

[a] Ceramic Physics Laboratory and Research Institute for Nanoscience, Kyoto Institute of Technology, Sakyo-ku, Matsugasaki, 606-8585 Kyoto, Japan
[b] Department of Medical Engineering for Treatment of Bone and Joint Disorders, Osaka University, 2-2 Yamadaoka, Suita, Osaka 565-0854, Japan

ARTICLE INFO

Article history:
Received 13 August 2010
Received in revised form 12 October 2010
Accepted 13 October 2010
Available online 18 October 2010

Keywords:
Polarized Raman analysis
UHMWPE
Residual strain
Molecular orientation
Tibial insert

ABSTRACT

The response to applied strain of EtO-sterilized and γ-irradiated polyethylene materials belonging to tibial inserts has been studied by polarized Raman spectroscopy. Initial calibrations on as-received samples from three different makers were employed to clarify the rearrangement of molecular chains under strain, expressed in terms of Euler angular displacements in space and orientation distribution functions. This body of information was then applied to a quantitative analysis of four tibial inserts (from the same three makers of the unused samples) retrieved after in vivo exposures ranging between 7 months and 5 years 8 months. The main results of the Raman analysis can be summarized as follows: (i) γ-irradiated samples experienced lower texturing on the molecular scale compared to EtO-sterilized samples, likely due to a higher strain recovery capability; and (ii) independent of sterilization method, the amount of plastic strain was mainly developed early after in vivo implantation, whereby out-of-plane molecules rotated under load onto planes parallel to the sample surface until saturation of angular displacements was reached.

1. Introduction

Surgeons and technologists make daily attempts to improve the outcome of total knee arthroplasty (TKA), with the ultimate goal of implanting prostheses that will reliably last as long as a human lifetime. Their main objectives reside in avoiding mechanical failure of ultrahigh-molecular-weight polyethylene (UHMWPE) bearings and in vivo generation of polyethylene debris, which are unquestionably the most commonly encountered issues affecting the durability of joint replacements [1,2]. The cyclic sliding motion between femoral condyle and polyethylene tibial insert components induces wear and fatigue damage that can lead to separation of micrometric particles of polyethylene from the surface or even, in the most unfortunate cases, to fracture of the bearing parts [1–5]. The subproducts of wear degradation are the most common causes of failure for bearing components embedded in the human body, since the body reacts to the presence of such foreign particles with a kind of bone degeneration, referred to as osteolysis, which leads to the need for revision surgery [6–9]. Even if the knee joint forces are comparable to those at the hip cup, due to the non-conformity between the surfaces of the tibial and femoral components, the external cyclic load applied to the tibial plate is distributed over a more limited area than the hip, generating a level of stress that could easily exceed the polymer yield strength [10,11]. Therefore, building a clear picture of the structural changes occurring during in vivo loading in the "soft" components of artificial knees represents a necessary step to understanding and improving TKA procedures.

The texture of a structurally complex material like biomedical polyethylene, namely the orientation distribution of crystalline lamellae and molecular chains, has been studied at great depth [12–14]. Such microstructural features play a crucial role in both wear resistance and strength properties. Several studies can be found in the literature that report about structural modifications induced by the processing of polyethylene components. For example, samples produced by extrusion and by compression molding have been studied extensively in the past few decades and the microstructural features uncovered are proof that texture can be introduced into a polymer structure as a consequence of plastic deformation.

Bellare and Cohen [14] determined the nature of the crystallographic texture in ram-extruded rod stock and compression-molded sheets of UHMWPE used in joint replacement prostheses. These processing steps themselves induce a crystallographic texture in the polymer structure, but the extent of such a texture formation is not comparable to that occurring under large plastic deformation. Nevertheless, the preferential orientation of molecular chains can be noticed as a consequence of crystallization in oriented polyethylene melt under normal compressive stress.

* Corresponding author. Tel./fax: +81 0 75 724 7568.
E-mail addresses: pezzotti@kit.ac.jp, pezzotti@chem.kit.ac.jp (G. Pezzotti).

1742-7061/$ - see front matter © 2010 Acta Materialia Inc. Published by Elsevier Ltd. All rights reserved.
doi:10.1016/j.actbio.2010.10.014

Song et al. [15] investigated samples of high-density polyethylene (HDPE) produced either by rolling or by channel-die compression. The orientation of orthorhombic crystallographic planes was evaluated by means of wide- and small-angle X-ray scattering (WAXS and SAXS, respectively), and a preferential distribution of *c*-axis along the plastic flow direction was noticed. Moreover, the tendency of the orthorhombic *a*-axis to orient toward the loading direction was reported.

The microstructural modifications induced by uniaxial compression in HDPE have also been studied by Bartczak et al. [16] at different stages of deformation using WAXS and SAXS, in addition to transmission electron microscopy (TEM). In this latter study, the change in the morphology of the polymer structure was monitored at values of true strain up to 2. As revealed by TEM micrographs, the initial spherulitic superstructure was completely random and, during deformation, the lamellae rotated away from the loading direction. Moreover, from the very beginning of the plastic deformation process, a tendency of the *a*-axis to align along the loading direction was confirmed.

In this study, we build upon our previously published study of molecular orientation in biomedical polyethylene materials for acetabular cups of hip joints [17] and use polarized Raman microspectroscopy to quantitatively assess the microstructural modifications induced by plastic deformation in polyethylene bearing components used in TKA. Tibial inserts that had undergone plastic deformation (in addition to that initially stored in the samples upon processing) in vivo were analyzed, and compared with the respective unused samples as received from the makers. In order to take into account the effect of the initial state on the molecular scale of the different polyethylene structures investigated, samples taken from unused tibial plates were first subjected to uniaxial compression tests and the evolution of their structural texture during plastic deformation monitored for each type of material investigated. Upon collecting polarized Raman spectra at different values of residual compressive strain, the rearrangement of the different molecular structures was assessed and expressed quantitatively by invoking a mathematical description of the molecular orientation based on both Raman selection rules and orientation distribution functions (ODFs) [18–20]. By so doing, the plastic strain stored in the material could be correlated with the out-of-plane variation of the tilt angle in the polyethylene chains and the variation of the statistical ODF parameters. Based on these results, retrieved knee joints produced by different manufacturers and sterilized by different methods could be analyzed quantitatively and the structural modifications induced in vivo upon plastic deformation clarified and discussed comparatively.

2. Materials and methods

A total of seven UHMWPE tibial plates were characterized, three as received from the makers and four retrieved after TKA revision surgery. Of the four retrieved UHMWPE tibial plates, two were manufactured by Japan Medical Materials (JMM, Osaka Japan) and sterilized by ethylene oxide (EtO) gas (henceforth referred to as samples A and B), while the remaining two, referred to as samples C and D, were commercially distributed by Stryker K.K. (Tokyo, Japan) and Smith and Nephew Orthopedics (Tokyo, Japan), respectively. The tibial plate C was vacuum/N_2 flush packaged, then γ-irradiated (33 kGy), while plate D was sterilized with EtO. Sample A belonged to a 73-year-old female patient for which the cause of revision was aseptic loosening with a follow-up period of 5 years 8 months. Sample B belonged to a 77-year-old female patient. For this latter patient, the cause of revision was also aseptic loosening after a follow-up period of 4 years 7 months. Samples C and D were retrieved from female patients whose ages were 83 and 81 years, respectively. In the former case, the cause of revision was aseptic loosening after an implantation period of 4 years, while for the latter the cause was malpositioning after a follow-up of only 7 months. All patients were old and not very active, though all were ambulators. Table 1 gives a summary of the investigated cases, including manufacturing characteristics and clinical data. The three unused tibial plates were of the same type as the retrieved ones, one from each manufacturer. All three types of tibial plate were machined from compression-molded sheets. We shall henceforth use the same letters for the as-received samples as for the retrieved plates, thus indicating manufacture by the same maker.

Raman spectra were collected at room temperature by means of a triple monochromator (T-64000, Jovin-Ivon/Horiba Group, Kyoto, Japan) equipped with a charge-coupled device detector, and analyzed with commercially available software (Labspec, Horiba/Jobin–Yvon, Kyoto, Japan). The excitation source was an Ar-ion laser operating at 488 nm. The spectral integration time was typically 20 s, with the recorded spectra being averaged over three successive measurements at each selected location. The samples were probed on their surfaces by visually selecting the locations under an optical microscope. Twenty locations for Raman assessments were randomly selected in both the main wear and non-wear zones of each in vivo exposed tibial plate. In order to minimize the in-depth convolution of the Raman information (which can be significant due to the high transparency of polyethylene to visible light), a 100 μm confocal pinhole was used. In this way, the probe size could be confined to 2.2 and 6.4 μm in plane and in depth, respectively. Further details of the stereological configuration of the confocal probe and its response function have been published elsewhere [21].

Structural modifications induced by plastic deformation in a uniaxial compression jig were preliminarily characterized and calibrated on unused tibial plates of the same types as the retrievals. In these calibration experiments, samples were cut from tibial inserts as received from the makers in order to obtain rectangular bars. Since the investigated retrievals were produced by different manufacturing processes and sterilized by different methods, it was expected that the polymer microstructures would differ and the response to applied stress would be strongly influenced by the processing circumstances. In particular, unlike EtO sterilization, γ-irradiation is known to generate cross-linking and, concurrently, to produce free radicals [21–24]. Such major alterations of the polymeric structure are known to strongly affect the macroscopic strain behavior. For this reason, calibrations under compressive load were repeated for each type of tibial insert. Twenty locations were randomly selected for each unused sample at each level of applied plastic strain. Fig. 1a shows the dimensions of the samples and the location in the unused tibial components from which the samples for uniaxial testing were obtained. The cut configuration was chosen so as to represent as much as possible the conditions of in vivo loading. Particular care was taken in order to cut the tibial insert in a position in which the bearing surface is almost parallel (misalignment always <4°) to the lower surface of the insert itself. Moreover, the effect of the curvature upon loading the 3×3 mm square face obtained after cutting was in this case negligible. The surface of the sample was then investigated by confocal Raman spectroscopy (Fig. 1b). For each type of tibial insert, two rectangular bars were loaded at different steps. As previously mentioned, each data point in the plots shown in the remainder of this paper was calculated from a value averaged over 20 locations (i.e. each one was analyzed with a probe 2.2 μm in width and 6.4 μm in depth) for each investigated strain value. The compressive load was applied parallel to the long axis of the sample (i.e. as in the case of in vivo loading) by means of a uniaxial compressive jig described in a previous study [25]. In order to as-

Table 1
Manufacturing characteristics and clinical data of the four retrievals investigated.

	Marker/name of implant	Resin	Processing	Sterilization	Size	Patient	Follow-up	BMI
Case A	JMM/KU3	GUR 1050	Compression moulding	EtO	Small 9 mm	73 years female	5 years 8 months	22.0
Case B	JMM/KU3	GUR 1050	Compression moulding	EtO	X-small 9 mm	77 years female	4 years 7 months	23.6
Case C	Stryker/scorpio NRG	GUR 1020	Compression moulding	γ-ray (33 kGy)	8 mm with stabilizer	83 years female	4 years	23.1
Case D	Smith and Nephew/genesis II	GUR 1020	Compression moulding	EtO	9 mm H/F	81 years female	7 months	25.8

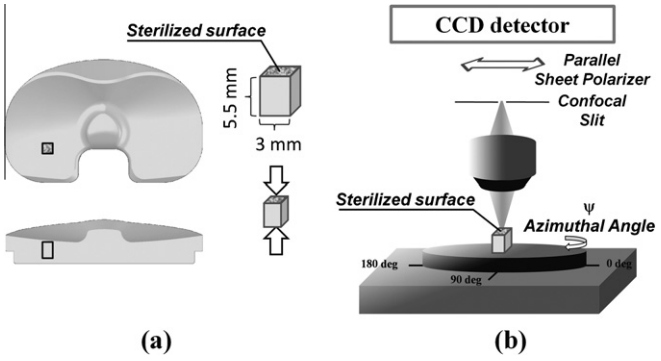

Fig. 1. (a) Geometry of the samples and the location in the unused tibial components from which they were extracted for performing uniaxial strain testing. A compressive load was applied parallel to the long axis of the sample. (b) A schematic draft of the experimental set-up adopted for in-plane rotation assessments. Raman spectra were collected using sheet polarizers in parallel configuration with respect to the incident laser polarization vector and filtered by means of a confocal pinhole placed across the backscattered emission.

sess only the plastic component of the strain, after each step of compression, we left the sample unloaded for 24 h until a complete recovery of the anelastic strain component in the polymer structure was achieved. The compressed surface was analyzed with placing the sample in a rotation jig and collecting polarized Raman spectra at different azimuthal angles, ψ. In Fig. 1b, a schematic draft is shown that explains the experimental set-up adopted for in-plane rotation assessments. Raman spectra were collected using sheet polarizers in parallel configuration with respect to the incident laser polarization vector. Particular care was taken to align the axis of the microscope with the axis of the rotation jig. For each point under investigation, Raman polarized spectra were collected at 19 different azimuthal angles within the interval $0^\circ \leqslant \psi \leqslant 180^\circ$, with sequential steps of 10°. The same procedure was adopted to analyze both wear zones and non-wear zones in the retrieved tibial plates.

Deconvolution of the polarized Raman spectra into elementary sub-bands was performed according to an automatic fitting algorithm within in a commercially available computational package (Labspec 3, Horiba/Jobin–Yvon, Kyoto, Japan). Mixed Gaussian/Lorentzian curves were used throughout the spectral fitting computations. Mathematical data treatment, according to the theory described in the following section, was performed with the aid of commercially available software (Mathematica 4; Wolfram Research Inc., IL, USA).

3. Theoretical assessment

This section represents the theoretical backbone of the paper, which we consider to be an original contribution to the field. Readers who are not interested in theory can go directly to the next section (Section 4), which is written with the purpose of being understandable even without a detailed reading of the theoretical part.

Polyethylene is a semicrystalline polymer that can be summarily described as a two-phase composite with crystalline lamellae embedded in an amorphous matrix [26]. The molecular chains of the crystalline phase can orient themselves into a highly ordered structure whose unit cell is mainly orthorhombic with lattice constants of **a** = 0.74 nm, **b** = 0.493 nm and **c** = 0.254 nm [27]. The fraction of crystalline phase, α_c, embedded in the amorphous matrix can be assessed quantitatively from the relative intensity of selected Raman bands, according to the procedure given by Mutter et al. [28], which we have also extensively applied in our previous studies of biomedical grades of polyethylene [17,21]. As far as the molecular orientation of the crystalline lamellae is concerned, the tensorial rules governing the relative intensity of Raman bands for the orthorhombic crystal structure can be expressed as functions of Euler angles in space and probe polarization geometry [29,30], by expanding the following tensorial equation:

$$I \propto |e_i \Re e_s|^2 \tag{1}$$

where I represents the scattered Raman intensity; e_i and e_s are the unit polarization vectors of the electric field for incident and scattered light, respectively. For a fixed polarization vector of the incident light (which is the case of our Raman equipment), parallel and cross-polarization geometries are thus possible for the scattered light. A full expansion of Eq. (1) in the case of UHMWPE has been published previously [17] so, for brevity's sake, it is not repeated here. In this study, we evaluated the preferential orientation of polyethylene molecules considering the Raman band located at 1130 cm^{-1} related to the C–C stretching vibration ($A_g + B_{1g}$ mode). The unit polarization vectors can be expressed in Cartesian coordinates as follows:

$$e^{\parallel}_{i\ xyz} = (0 \quad 1 \quad 0), \quad e^{\parallel}_{s\ xyz} = \begin{pmatrix} 0 \\ 1 \\ 0 \end{pmatrix} \tag{2}$$

where the subscripts i and s refer to incident and scattered light, respectively; the superscript $\parallel$ indicates parallel polarization (i.e. $Z(YY)\overline{Z}$ in Porto notations [31]). $\Re$ represents the second-rank Raman scattering tensor of the vibrational mode under consideration. The Raman tensor expressed in the Cartesian frame of the principal crystal axis for the A_g and B_{1g} mode are given as [32]:

$$\Re_{A_g} = \begin{pmatrix} a & 0 & 0 \\ 0 & b & 0 \\ 0 & 0 & c \end{pmatrix} \quad , \Re_{B_{1g}} = \begin{pmatrix} 0 & d & 0 \\ d & 0 & 0 \\ 0 & 0 & 0 \end{pmatrix} \tag{3}$$

Rearranging Eqs. (1)–(3), the dependence of the Raman intensity on the crystallographic orientation in parallel polarization can be explicitly expressed in terms of three Euler angles in space after rotation of the Cartesian frame, as follows [17,33]:

$$\begin{aligned} I^{\parallel}_{A_g+B_{1g}} = \Lambda \Big\{ \alpha_c \Big[& c \sin^2\theta \sin^2\psi + a(\sin\varphi\cos\psi + \cos\theta\cos\varphi\sin\psi)^2 \\ & + b(\cos\varphi\cos\psi - \cos\theta\sin\varphi\sin\psi)^2 \Big]^2 \\ & + (1-\alpha_c)[-2d(\sin\varphi\cos\psi + \cos\theta\cos\varphi\sin\psi)(\cos\varphi\cos\psi \\ & + \cos\theta\sin\varphi\sin\psi)]^2 \Big\} + \Gamma \end{aligned} \tag{4}$$

In Eq. (4), Λ and Γ represent numerical constants that depend on the instrumental configuration and on the spectral band employed; as already mentioned, α_c is the crystallinity fraction

present in the composite polymeric structure, which can be obtained from the relative intensity of selected Raman bands [21]. The Raman tensor parameters for the orthorhombic structure of polyethylene ($a = -0.762$, $b = -0.944$, $c = 0.240$ and $d = -0.403$) along with Λ and Γ (these latter two parameters depending on the experimental configuration of the optical instrument) have been determined in previous papers [17,33]. It should be noted that, when dealing with highly textured materials (e.g. polyethylene fibers [33]), the application of Eqs. (1) and (4) in Raman analysis is straightforward; however, a more complex approach is needed to describe partly aligned microstructures. In order to obtain a fully quantitative assessment of the stereological character of molecular textures, local ODFs also need to be taken into consideration in the computational routine, because only a fraction of the full molecular population is aligned. The structure of the ODF has been formulated in terms of Wigner functions using a formalism of polynomial expansion in series of Legendre [34–37]. Fig. 2 shows our choices of Cartesian systems, as follows: a Cartesian system (*XYZ*) integer to the laboratory, a Cartesian system (*xyz*) integer to the molecular orientation axes (i.e. with its *z*-axis parallel to the long axis of the molecular chain) and an additional Cartesian system ($x_{mol}y_{mol}z_{mol}$) locating the molecular orientation axes within the polarized Raman probe. The axes of preferential orientation of the molecular structure were labeled ($x_p y_p z_p$), with z_p corresponding to the *c*-axis of the molecular frame. As far as different sets of Euler angles are concerned (cf. Fig. 2), the set of angles (θ, φ, ψ) locates the orientation in space of an arbitrary polyethylene molecule (i.e. located by (*xyz*)) with respect to the Cartesian system (*XYZ*); the set of angles (α, β, γ) instead describes the rotations in space of the Cartesian frame integer to the molecular orientation axes, ($x_{mol}y_{mol}z_{mol}$), within the polarized Raman probe, with respect to the axes of preferential orientation of the molecular structure, ($x_p y_p z_p$). In addition, the set of Euler angles describing the rotations of the preferential orientation axes, ($x_p y_p z_p$), of the molecular chains with respect to the laboratory frame (*XYZ*) were labeled $(\theta_p, \varphi_p, \psi_p)$. According to the above notations, the three Euler angles (θ, φ, ψ) describing the orientation of any arbitrary molecule in space with respect to the laboratory Cartesian system, (*XYZ*), can be expressed as functions of α, β, θ_p, φ_p and ψ_p by considering a double matrix rotation, as explicitly shown in the Appendix.

Upon considering φ as a constant equal to φ_p in our calculations, namely neglecting any torsional rotations of the molecular chains around their *c*-axis, a working equation that includes both Raman selection rules and molecular distribution patterns can be set, as follows [17,33]:

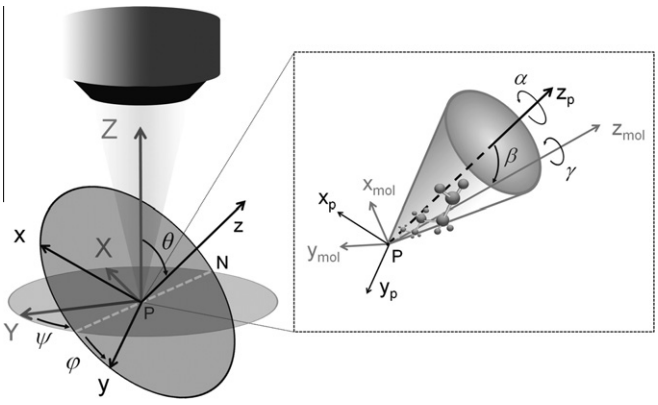

Fig. 2. Schematic draft of our choice of Cartesian reference systems and of the Euler angles (θ, φ, ψ) governing their rotations in space, as explained in the text.

$$I^{\parallel}_{A_g}(\theta,\varphi,\psi) = \frac{\int_{\gamma=0}^{\gamma=2\pi}\int_{\alpha=0}^{\alpha=2\pi}\int_{\beta=0}^{\beta=\pi} I^{\parallel}_{A_g+B_{1g}}(\theta,\varphi,\psi) f(\beta)\sin\beta d\beta d\alpha d\gamma}{\int_{\gamma=0}^{\gamma=2\pi}\int_{\alpha=0}^{\alpha=2\pi}\int_{\beta=0}^{\beta=\pi} f(\beta)\sin\beta d\beta d\alpha d\gamma} \quad (5)$$

with the polarized Raman intensity, $I^{\parallel}_{A_g+B_{1g}}(\theta,\varphi,\psi)$, given by Eq. (4). The orientation distribution function, $f(\beta)$, is then given as [34–37]:

$$f(\beta) = A\exp\{-[\lambda_2 P_2(\cos\beta) + \lambda_4 P_4(\cos\beta)]\} \quad (6)$$

where *A* is a constant and the parameters λ_2 and λ_4 are the Lagrange multipliers used in the definition of the principle of maximum information entropy reported by Pérez et al. [37] and Jaynes [38]. Note that in the computational process we excluded in first approximation any azimuthal dependence of the orientation distribution function, which is thus taken to be dependent only on the polar angle, β (i.e. assuming the existence of a uniaxial symmetry with respect to the preferential orientation of the molecular chains). Experimental Raman intensities collected upon rotation of the probe volume enable Eq. (5) to be set (i.e. after substituting for the variables θ and ψ from Eqs. (A4) and (A5)) at each of the *n* selected in-plane rotation angles, ψ, thus obtaining a system of *n* independent equations that can be numerically solved by means of an iterative numerical routine. Note that the number *n* of selected ψ angles, and thus the number of independent equations, should exceed the number of unknown parameters (in this case, five: θ_p, φ_p, ψ_p, λ_2 and λ_4). Given the high number of variables involved in the integration, and the large number of collected points in the polyethylene structure, the computation can be quite time consuming (it required several weeks in our case). In the interval, $0 \leqslant \psi \leqslant \frac{\pi}{2}$, we collected $n = 10$ relative intensity values at each investigated location, which greatly exceeded the number of unknown parameters. From any five independent equations, we obtained the unknown parameters, θ_p, φ_p, ψ_p, λ_2 and λ_4, according to a best fitting procedure, while using the remaining equations for a confirmation of the obtained values. Lagrange multipliers calculated by the aforementioned fitting procedure enabled us to determine the three parameters *A*, $\langle P_2(\cos\beta)\rangle$ and $\langle P_4(\cos\beta)\rangle$ by solving a system of three additional equations, as follows [17,33]:

$$\int_{\gamma=0}^{\gamma=2\pi}\int_{\alpha=0}^{\alpha=2\pi}\int_{\beta=0}^{\beta=\pi} f(\alpha,\beta,\gamma)\sin\beta d\beta d\alpha d\gamma = 1 \quad (7)$$

$$\int_{\gamma=0}^{\gamma=2\pi}\int_{\alpha=0}^{\alpha=2\pi}\int_{\beta=0}^{\beta=\pi} P_2(\cos\beta) f(\beta)\sin\beta d\beta d\alpha d\gamma = \langle P_2(\cos\beta)\rangle \quad (8)$$

$$\int_{\gamma=0}^{\gamma=2\pi}\int_{\alpha=0}^{\alpha=2\pi}\int_{\beta=0}^{\beta=\pi} P_4(\cos\beta) f(\beta)\sin\beta d\beta d\alpha d\gamma = \langle P_4(\cos\beta)\rangle \quad (9)$$

Of the two "order parameters", $\langle P_2(\cos\beta)\rangle$ and $\langle P_4(\cos\beta)\rangle$, the former is referred to as Herman's orientation parameter [36]. This parameter assumes the value 0 when the molecular orientation is fully random, while values 1 and −0.5 are experienced when a perfect orientation is reached parallel and perpendicular to a preferential orientation axis, respectively. Herman's orientation parameter is the primary parameter in judging the alignment of polyethylene chains [37]. In this study, the calculated value of θ_p represents the out-of plane tilt angle with respect to the loaded surface of the polyethylene bearing. This angle thus directly represents the microstructural modification induced in the polymeric structure by a compressive strain field applied along a direction perpendicular to the bearing surface. Out-of-plane angular displacements should be distinguished from variations of in-plane angle, ψ_p, which, in a previous study [17], were related to molecular displacements taking place on the surface of the bearings (i.e. at the contact point), owing to the development of frictional forces.

4. Results and discussion

4.1. Molecular rearrangement under uniaxial strain

In this section, we show preliminary strain calibration procedures, in which we monitored the polyethylene microstructures from its as-received state (i.e. at residual strain assumed as $\varepsilon = 0$) up to $\varepsilon = 12\%$ of uniaxial compressive true strain. Since there was no appreciable difference between the behaviors of the two EtO-sterilized materials produced by the different makers, we shall show and discuss the strain calibration results by simply comparing EtO-sterilized and γ-irradiated samples. Examples of experimental angular dependencies obtained upon in-plane rotation at different stages of uniaxial deformation for EtO-sterilized samples are shown in Fig. 3a, while the results of best fitting and the calculated ODFs are reported in Fig. 3b and c, respectively. Similarly, experimental results of polarized Raman intensity as a function of in-plane rotation, the related best fitting curves and ODFs are reported for the γ-irradiated sample in Fig. 3d–f, respectively. The Raman selection rule, given by Eq. (4) for the $A_g + B_{1g}$ mode, invariably shows that the periodicity of the Raman intensity fluctuation should be expected over an angular interval $0 \leqslant \psi \leqslant \pi$ and that the maximum intensity corresponds to a given preferential (in-plane) orientation of the molecular chains (i.e. corresponding to the azimuthal angle, ψ_p). The plots in Fig. 3a, b, d and e indeed confirm that such a preferential orientation exists with periodicity π. Such a trend is independent of uniaxial strain applied along a direction perpendicular to the sample surface. Independent of the adopted sterilization procedure, the in-plane Euler angle locating the preferential orientation on the surface of the sample was measured as $\psi_p \approx \frac{\pi}{5}$ and was invariant with increasing magnitude of applied (static) strain. On the other hand, as a general rule, an increase in applied strain led to a larger population of molecular chains experiencing preferential orientation, as shown by the increasingly pronounced maximum in the calculated ODF (cf. Fig. 3c and f for EtO-sterilized and γ-irradiated materials, respectively). However, such a trend appeared more pronounced in the EtO-sterilized material compared to the γ-irradiated one. Important to the present context is that the experimental plots in Fig. 3 also contain information about the out-of-plane molecular orientation angle, θ_p. Fig. 4 shows values of θ_p and Herman's parameter, $\langle P_2(\cos\beta)\rangle$, as retrieved from the best fitting of the full set of strain dependence curves (of which a selection is shown in Fig. 3b and e for EtO-sterilized and γ-irradiated samples, respectively). The salient notions that can be extracted from the plots in Fig. 4 are summarized as follows: (i) the molecular chains are initially aligned along a direction nearly perpendicular ($\theta_p \approx \frac{\pi}{12}$) to the sample surface in a similar way for both types of sample, although commonly with a low statistical frequency ($\langle P_2(\cos\beta)\rangle \approx 0.25$); (ii) the tilt angle, θ_p, locating the direction of the long axis of the molecular chains gradually increases up to $\theta_p \approx \frac{\pi}{5}$ (with a slope similar for both types of material) under application of strain; and (iii) unlike the γ-irradiated sample, which showed a comparatively low statistical degree of alignment ($0.25 \leqslant \langle P_2(\cos\beta)\rangle \leqslant 0.4$)

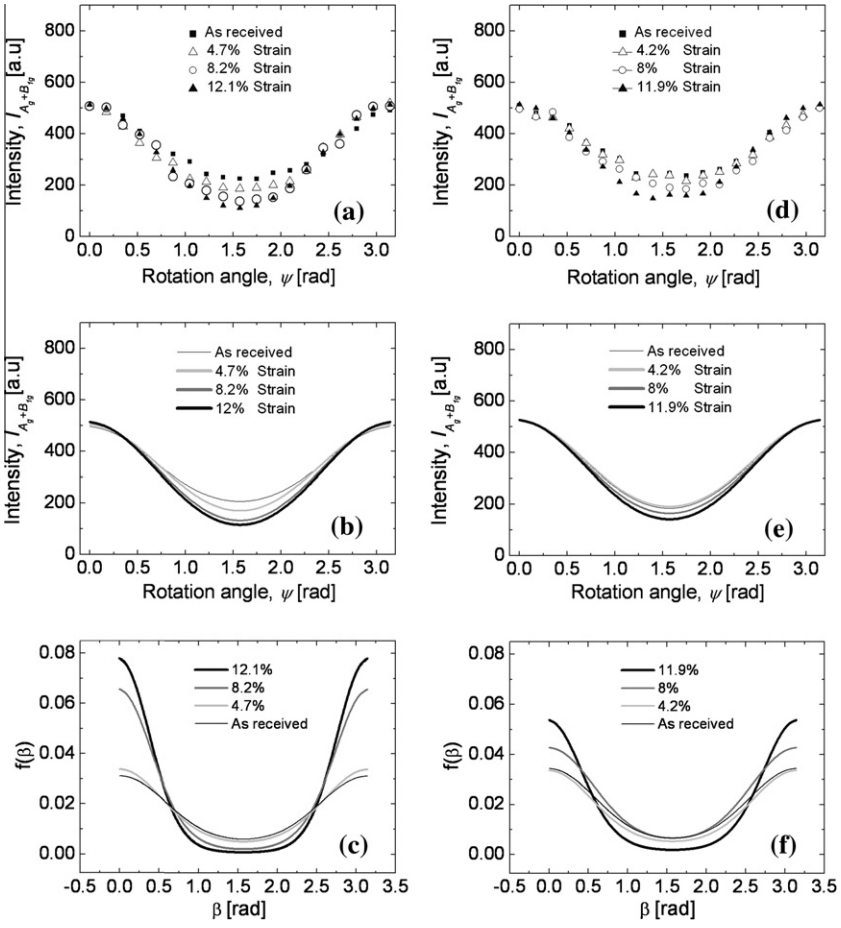

Fig. 3. Experimental azimuthal angular dependencies obtained upon in-plane rotation at different stages of uniaxial deformation for EtO-sterilized samples (a). The results of best fitting to the experimental data and the calculated ODFs are reported in (b) and (c), respectively. Analogous plots are also shown for the case of the γ-irradiated sample in (d)–(f), respectively.

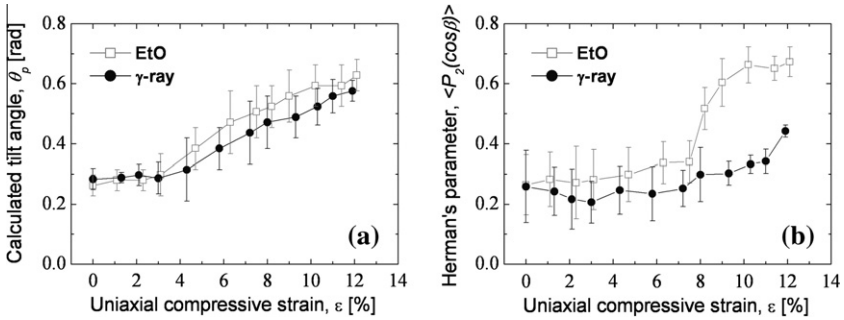

Fig. 4. Values of (a) θ_p and (b) Herman's parameter, $\langle P_2(\cos\beta)\rangle$,as retrieved from the best fitting curves as shown in Fig. 3b and e for EtO-sterilized and γ-irradiated samples, respectively. Error bars represent the standard deviations of the measurements.

over the entire interval of investigated strain, the EtO-sterilized sample showed an abrupt increase in Herman's parameter (i.e. up to $\langle P_2(\cos\beta)\rangle \approx 0.7$), starting from a threshold value of strain at around 7.5%.

As far as the above point (i) is concerned, the finding is in agreement with the study of Bellare and Cohen [14] on compression-molded sheets, a similar angular population for EtO-sterilized and γ-irradiated samples in their as-received state conceivably arising from the samples being manufactured from rods obtained by the same procedure. It is also reasonable that uniaxial strain tends to align the molecular chains in a direction parallel to the surface, i.e. perpendicular to the direction of the applied compressive load. Galeski et al. [39] presented a comprehensive interpretation of the morphological alteration of the polyethylene structure during plane strain compression. At the initial stage of deformation, the main mechanism of structural rearrangement was described as consisting mainly of interlamellar sliding, while chain slip within individual crystallites becomes active at a subsequent stage, when the lamellae start "feeling" shear strain and molecular chains become prone to slip along the [0 0 1] direction of the orthorhombic structure (corresponding to a slip along the most closely packed crystallographic plane). At higher deformation levels, the lamellae are more and more elongated and a decrease in thickness is also observed. This latter structural modification is due to the movement of chains, which are forced to align along the direction of plastic flow. It has been postulated that, at rather elevated levels of strain, the microstructure of polyethylene can develop a texture that is similar to that of a single crystal [40].

According to our results (cf. trends of θ_p angles in Fig. 4), the onset strain for obtaining a modified texture is ~3–4% for EtO-sterilized UHMWPE, while in γ-irradiated polyethylene such a strain threshold seems to be somewhat raised (or, for the same strain threshold, the θ_p gradient is appreciably lower). This observation, together with the different trends of ODF (cf. Fig. 3c and f) between γ-irradiated and EtO-sterilized polyethylene, might confirm the findings of Bartczak [41] and Boontongkong et al. [42], which can be summarized as follows. Highly entangled and highly cross-linked polyethylene achieve higher crystallographic orientation when subjected to the same strain as less cross-linked and/or less entangled polyethylene. This is because the initial deformation accommodated by the amorphous regions below the yield stress results in macromolecules getting extended and "locked" prior to activation of slip systems in the lamellar regions. If the polyethylene is cross-linked then it gets fully stretched to its maximum limit at lower strains and begins to reorient the lamellae. Thus macromolecular orientation is faster (at lower strains) in cross-linked polyethylene. The observations of this study that irradiated polyethylene has lower orientation is not a result of lower molecular mobility but probably because, upon unloading, highly cross-linked and/or more entangled polyethylene has a higher strain recovery than polyethylene that is less entangled and has lower or no cross-linking. Presumably, during the initial stage of plastic strain, only the amorphous phase undergoes plastic deformation, while the crystalline orthorhombic phase becomes involved with the structural rearrangement process only at higher values of strain. During the secondary deformation stage, i.e. in the range of ε between 4% and 12%, we observed the most remarkable variation of the out-of-plane tilt angle, θ_p, which suggests that the observed strain threshold is related to a homogeneous tendency of orthorhombic molecules to align along a plane parallel to the sample surface.

The observed trends of molecular rearrangement in both types of sample can be rigorously expressed according to phenomenological curves, $\varepsilon = \varepsilon(\Delta\theta_p)$, as shown in Fig. 5a and b for EtO-sterilized and γ-irradiated samples, respectively. The $\Delta\theta_p$ trends represent the variation of out-of-plane tilt angle with respect to the original orientation direction before loading. The plots in Fig. 5 are different for EtO and γ-irradiated materials; however, a procedure of least-squares fitting led to two equations of a common cubic nature, as follows:

$$\varepsilon = 71.96\Delta\theta_p - 302.72\Delta\theta_p^2 + 546\Delta\theta_p^3 \quad (10)$$

$$\varepsilon = 119.47\Delta\theta_p - 643.82\Delta\theta_p^2 + 1293.28\Delta\theta_p^3 \quad (11)$$

(with angular variations expressed in radians) for the EtO- and γ-irradiated materials, respectively. The correlation factor R^2 obtained for the fitting of the experimental curves to cubic polynomials was 0.993 and 0.987 for Eqs. (10) and (11), respectively. Eqs. (10) and (11) are important since they link the residual strain stored in the sample to a measurable microstructural parameter (i.e. $\Delta\theta_p$), and will be used in the next section to quantitatively discuss the amount of residual strain stored in tibial inserts during in vivo exposure.

4.2. Residual strain stored on the surface of retrieved tibial plates

Investigating the molecular orientation in retrievals is quite a challenging computational problem because, unlike unused samples, which are only statically loaded, retrievals are concurrently subjected to compressive and frictional forces. It follows that local variations of ψ_p cannot be neglected and, thus, the computational analysis of Raman intensities (i.e. through Eq. (5)) upon in-plane sample rotation should be applied while considering the concurrent variations of two Euler angles, θ_p and ψ_p. However, in analyzing retrievals, we can now take advantage of the two phenomenological Eqs. (10) and (11) in order to quantify the amount of compressive residual strain stored in the retrieved tibial plates. The results of polarized Raman analysis of four retrievals (i.e. those listed in Table 1) are summarized in Figs. 6 and 7 in terms of in-plane and out-of-plane Euler angles (i.e. ψ_p and θ_p,

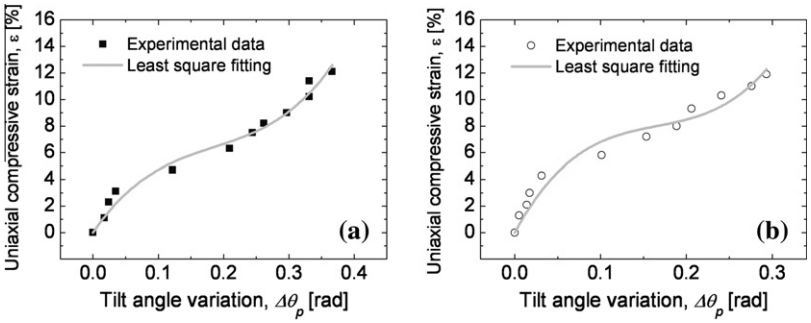

Fig. 5. Relationships between compressive strain and variation of out-of-plane tilt angle $\Delta\theta_p$ for EtO (a) and γ-ray (b) sterilized UHMWPE, respectively. Compressive residual strain is expressed as a function of $\Delta\theta_p$ by means of cubic interpolation functions. The least-squares fitting results led to Eqs. (10) and (11) for (a) and (b), respectively.

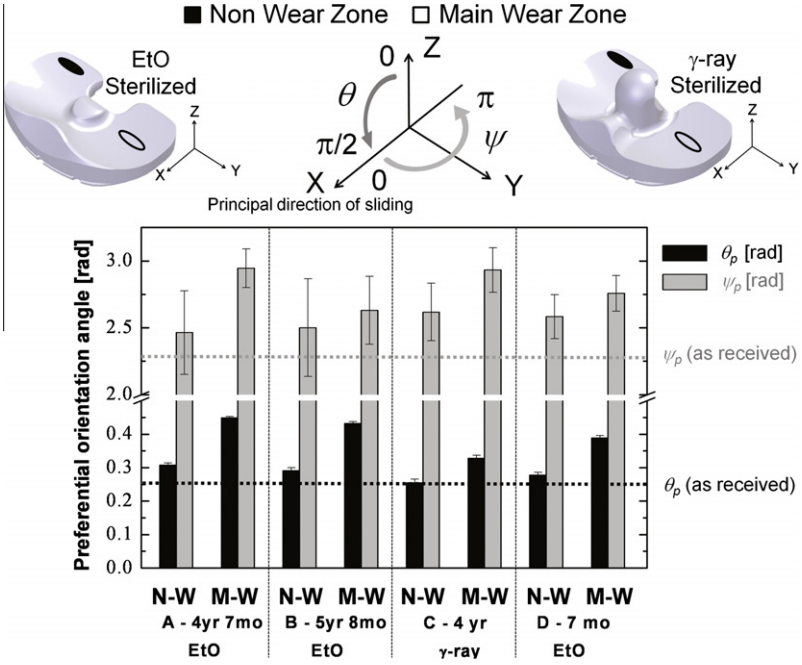

Fig. 6. Average preferential out-of-plane tilt angle, θ_p, and azimuthal in-plane angle, ψ_p, as calculated from the main wear zone and the non-wear zone of each of the four retrievals analyzed. The two dotted lines represent the average values of θ_p and ψ_p as obtained from virgin samples (as explained in the text, no significant difference was observed in the as-received samples due to the samples being prepared from the same resin). Error bars represent the standard deviations of the measurements.

describing the preferentially oriented long axis of the molecular chains) and residual strain, ε, respectively. Looking first at the data in Fig. 6, one can note that the θ_p values collected in the non-wear zones were all very close to the ψ_p and θ_p values observed in the unused plates (i.e. $\psi_p = \frac{\pi}{5}$ and $\theta_p \approx \frac{\pi}{12}$), independent of the sterilization process and as dictated by the common manufacturing process of the compression-molded sheets. In other words, the microstructures in the non-wear zone looked very much the same as those of the as-received samples, independent of exposure time in vivo and sterilization process. On the other hand, in the main wear zone of the retrieved tibial plates, locations at which the highest compressive and frictional loads were applied in vivo, the angles of molecular orientation, ψ_p and θ_p, showed appreciable changes with respect to the as-received state. In the three EtO sterilized samples, the tilt angle, θ_p, was found to commonly lie in a narrow interval at around $\frac{\pi}{8}$, despite the quite different exposure times in vivo (which was significantly shorter for sample D compared to samples A and B). The tilt angular rearrangement, $\Delta\theta_p \approx \frac{\pi}{22}$, for these three samples corresponds, according to Eqs. (10) and (11), to surface strains within a narrow range, $\varepsilon = 5.0 \div 5.5\%$ (cf. Fig. 7). This finding seems to confirm that the most significant amount of plastic deformation in polyethylene components occurs during the first year of implantation, as previously reported by other authors [43,44]. It should be noted that the load–displacement curves obtained by Edidin et al. [45] show higher strain hardening of GUR 1050 compared to GUR 1020. This means the relatively lower amount of residual plastic strain in sample D compared to samples A and B might be partly due to a difference in the type of resin.

Some residual strain seems also to accumulate in the non-wear zone, despite the conspicuously load-free conditions of such a part of the knee joint upon normal walking activity. Note that the conspicuous absence of wear in the non-wear zone during in vivo service does not necessarily mean an absence of load, which is the main cause of creep and thus molecular realignment. However, the calculated amount of residual strain is very low and within the experimental scatter. On the other hand, the γ-irradiated sample C, despite its comparatively long-term exposure in vivo, experienced quite low tilt angle variation for a similar amount of plastic strain (i.e. $\Delta\theta_p \approx \frac{\pi}{40}$ and $\varepsilon \approx 6\%$; cf. Figs. 6 and 7). This confirms the

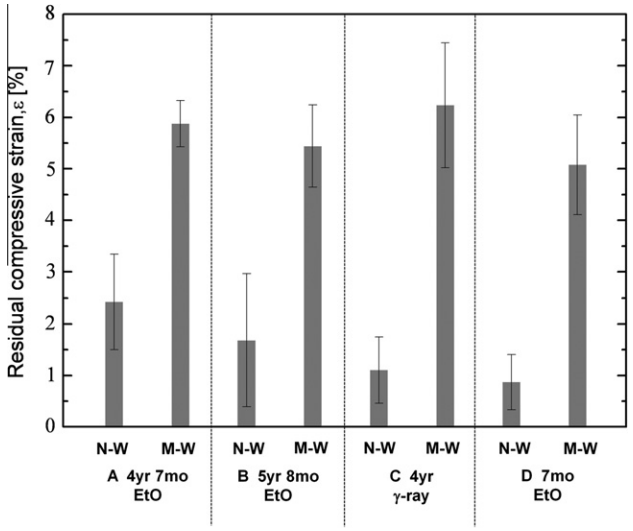

Fig. 7. Residual strain, ε, as calculated from the main wear and non-wear zones of the four retrievals investigated. Assessments were made using the phenomenological Eqs. (10) and (11). Error bars represent the standard deviations of the measurements.

higher strain hardening of the γ-irradiated sample as compared to the EtO-sterilized samples, which was also observed during static loading experiments.

Unlike the relatively straightforward outputs of the Raman analysis regarding the effect of compressive load on the surface of tibial insert retrievals, the analysis of in-plane molecular displacements appears to be more complex and difficult to rationalize. Thus, it might require a more comprehensive statistical approach, which we will attempt in a future study, when more retrievals are available. Sample A, for example, although being implanted for a period of time 13 months longer than sample B, showed less in-plane alignment along the direction of primary motion or the principal direction of sliding, as shown in Fig. 5 (i.e. $\psi = \pi$; cf. Fig. 6). It is indeed conceivable that, with longer periods of exposure time in vivo, the long axis of the polyethylene molecules tends to align on the surface in the direction of primary motion. Note that such a molecular alignment process has been reported to produce a partial reduction in wear resistance on the sample surface [46,47]. However, such a mobility process should strongly depend on both the level of activity and body weight of the patient. Unlike ψ_p angular displacements, clear differences could be found between ODFs calculated in the main wear zone and in the non-wear zone of each sample (Fig. 8a–d) for samples A, B, C and D, respectively). The plots in Fig. 8 were obtained considering the average ODF parameters for each investigated area, while Herman's parameters associated with each $f(\beta)$ distribution curve are explicitly shown in the inset to each plot. It should be noted that, although a preferential orientation of polyethylene chains has also been observed in non-wear zones, the distribution of molecular directions in these zones is always quite broad. On the other hand, by comparing the ODFs in the main wear zone of EtO-sterilized samples (i.e. samples A, B and D) with that of the γ-sterilized one (i.e. sample C), a significant difference can be found, thus confirming that γ-sterilized UHMWPE possesses a more "rigid" microstructure and, thus, is less prone to increase its degree of texture as a consequence of the occurrence of plastic deformation in vivo.

5. Conclusion

Polarized Raman spectroscopy has been quantitatively applied to determine the molecular rearrangements and the residual strain correlated to the plastic flow that occurs in vivo in tibial inserts of artificial knees. The Raman procedure was based on an improved analytical approach using ODFs, namely Wigner functions expressed in terms of Legendre polynomials, to describe the molecular population obeying a given set of Euler angles in space. Raman assessments based on this algorithm revealed clear changes in molecular orientation patterns in both the main wear and non-wear zones of tibial insert retrievals. Variations of out-of-plane and in-plane Euler angles, characteristic of the preferential orientation of the long axis of polyethylene chains, were found to mainly obey compressive and frictional forces, respectively. ODFs were

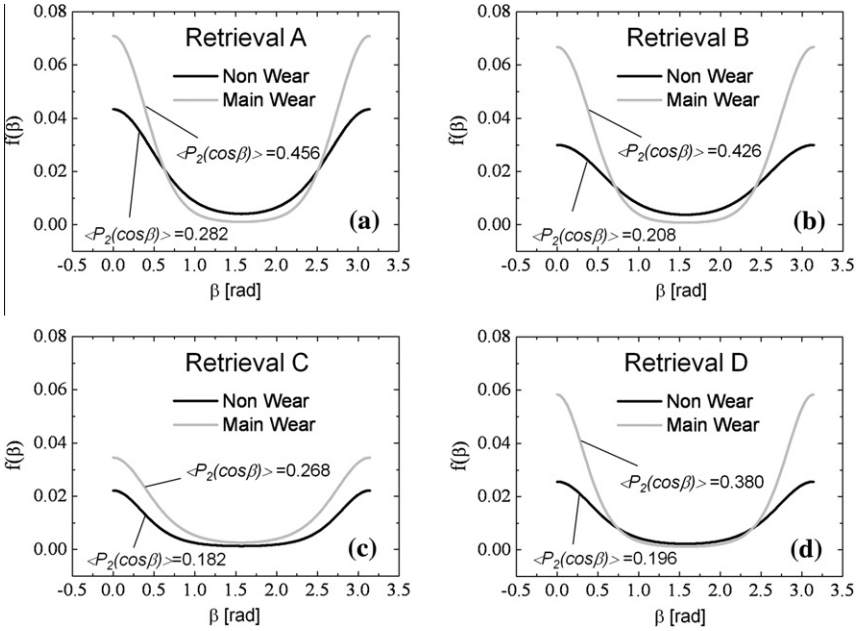

Fig. 8. ODFs calculated in the main wear zone and in the non-wear zone of each sample ((a), (b), (c) and (d) for samples A, B, C and D, respectively). Each plot was obtained by considering the ODF parameters averaged over the investigated area. Herman's parameters associated with each $f(\beta)$ distribution are explicitly shown in the inset to each plot.

proved to express suitably in quantitative terms structural parameters like molecular chain rearrangement and texture, which have hitherto only been discussed qualitatively in the majority of the literature regarding biomedical grades of polyethylene. It is understood that the present study has merely put forward a Raman methodology for analyzing retrieved tibial inserts; studies aimed at establishing the clinical performance of different implants must await the availability of a statistically meaningful number of retrievals and will be treated in forthcoming studies.

Appendix

The rotation matrices can be written as follows:

$$S = \begin{pmatrix} \cos\theta\cos\varphi\cos\psi - \sin\varphi\sin\psi & \cos\varphi\sin\psi + \cos\theta\cos\psi\sin\varphi & -\sin\theta\cos\psi \\ -\cos\theta\cos\varphi\sin\psi - \cos\psi\sin\varphi & \cos\varphi\cos\psi - \cos\theta\sin\varphi\sin\psi & \sin\theta\sin\psi \\ \sin\theta\cos\varphi & \sin\theta\sin\varphi & \cos\theta \end{pmatrix} \tag{A1}$$

$$M = \begin{pmatrix} \cos\theta_p\cos\varphi_p\cos\psi_p - \sin\varphi_p\sin\psi_p & \cos\varphi_p\sin\psi_p + \cos\theta_p\cos\psi_p\sin\varphi_p & -\sin\theta_p\cos\psi_p \\ -\cos\theta_p\cos\varphi_p\sin\psi_p - \cos\psi_p\sin\varphi_p & \cos\varphi_p\cos\psi_p - \cos\theta_p\sin\varphi_p\sin\psi_p & \sin\theta_p\sin\psi_p \\ \sin\theta_p\cos\varphi_p & \sin\theta_p\sin\varphi_p & \cos\theta_p \end{pmatrix} \tag{A2}$$

$$N = \begin{pmatrix} \cos\beta\cos\gamma\cos\alpha - \sin\gamma\sin\alpha & \cos\gamma\sin\alpha + \cos\beta\cos\alpha\sin\gamma & -\sin\beta\cos\alpha \\ -\cos\beta\cos\gamma\sin\alpha - \cos\alpha\sin\gamma & \cos\gamma\cos\alpha - \cos\beta\sin\gamma\sin\alpha & \sin\beta\sin\alpha \\ \sin\beta\cos\gamma & \sin\beta\sin\gamma & \cos\beta \end{pmatrix} \tag{A3}$$

where $S = s_{ij}$ $(i,j = 1,2,3)$ represents the rotations of (xyz) with respect to (XYZ), $M = m_{ij}$ $(i,j = 1,2,3)$ the rotations of $(x_p y_p z_p)$ with respect to (XYZ), and $N = n_{ij}$ $(i,j = 1,2,3)$ the rotations of $(x_{mol} y_{mol} z_{mol})$ with respect to $(x_p y_p z_p)$ (cf. Fig. 2). The matrix product $T = MN = t_{ij}$ $(i,j = 1,2,3)$ is equal to S, thus equating the elements $s_{33} = t_{33}$ and $s_{23} = t_{23}$. Two Euler angles can be then expressed as $\theta = \theta(\alpha, \beta, \theta_p, \varphi_p, \psi_p)$ and $\psi = \psi(\alpha, \beta, \theta_p, \varphi_p, \psi_p)$, as follows:

$$\theta = \arccos(\cos\beta\cos\theta_p - \cos(\alpha + \varphi_p)\sin\beta\sin\theta_p) \tag{A4}$$

$$\begin{aligned} \psi' = \arcsin\{&[\cos\alpha\cos\psi_p\sin\beta\sin\varphi_p \\ &+ \sin\psi_p\left(\cos\beta\sin\theta_p - \cos\theta_p\sin\alpha\sin\beta\sin\varphi_p\right) \\ &+ \cos\varphi_p\sin\beta(\cos\psi_p\sin\alpha - \cos\alpha\cos\theta_p\sin\psi_p)] \\ &/\sqrt{1 - \left(\cos\beta\cos\theta_p - \cos(\alpha + \varphi_p)\sin\beta\sin\theta_p\right)^2}\} \end{aligned} \tag{A5}$$

Appendix. . Figures with essential colour discrimination

Certain figures in this article, particularly Figure 6, are difficult to interpret in black and white. The full colour images can be found in the on-line version, at doi:10.1016/j.actbio.2010.10.014).

References

[1] Bergstrom JS, Rimnac C, Kurtz SM. Molecular chain stretch is a multiaxial failure criterion for conventional and highly crosslinked UHMWPE. J Orthop Res 2005;23:367–75.
[2] McDonald MD, Bloebaum RD. Distinguishing wear and creep in clinically retrieved polyethylene inserts. J Biomed Mater Res 1995;29:1–7.
[3] Kurtz SM, Muhlstein C, Edidin AA. Surface morphology and wear mechanisms of four clinically relevant biomaterials after hip simulator testing. J Biomed Mater Res A 2000;52(3):447–59.
[4] Wroblewski B. Direction and rate of socket wear in Charnley low friction arthroplasty. J Bone Joint Surg Br 1985;67B:757–61.
[5] Huber J, Walter A, Plitz W, Refior HJ. Effect of the manufacturing process on creep and wear properties of UHMWPE (ultra-high molecular weight polyethylene). Biomed Tech (Berl) 1995;40:88–92.
[6] Oparaugo PC, Clarke IC, Malchau H, Herberts P. Correlation of wear debris-induced osteolysis revision with volumetric wear rates of polyethylene. Acta Orthop Scand 2001;72(1):22–8.
[7] Zhu YH, Chiu KY, Tang WM. Polyethylene wear and osteolysis in total hip replacement. J Orthop Surg 2001;9(1):91–9.
[8] James SP et al. Challenge to the concept that UHMWPE acetabular components oxidize in vivo. Biomaterials 1993;14(9):643–7.
[9] Bankston AB, Cates H, Ritter MA, Keating EM, Faris PM. Polyethylene wear in total hip arthroplasty. Clin Orthop 1995;317:7–13.
[10] Kurtz SM. Stress in UHMWPE tibial and patellar components for TKR. In: Kurtz SM, editor. The UHMWPE handbook, ultra-high-molecular-weight-polyethylene in total joint replacement. New York: Elsevier Academic Press; 2002. p. 100–2.
[11] Bartel DL, Rawlinson VL, Burstein AH, Ranawat CS, Flynn Jr WF. Stress in polyethylene components of contemporary total knee replacements. Clin Orthop 1995;380:76–82.
[12] Olley RH, Hosier IL, Bassett DC, Smith NG. On morphology of consolidated UHMWPE resin in hip cups. Biomaterials 1999;20:2037–46.
[13] Li DS, Garmestani H, Alamo RG, Kalidindi SR. The role of crystallinity in the crystallographic texture evolution of polyethylenes during tensile deformation. Polymer 2003;44:5355–67.
[14] Bellare A, Cohen RE. Morphology of rod stock and compression-moulded sheets of ultra-high-molecular-weight polyethylene used in orthopaedic implants. Biomaterials 1996;17:2325–33.
[15] Song HH, Argon AS, Cohen RE. Morphology of highly textured high-density polyethylene. Macromolecules 1990;23:870–6.
[16] Bartczak Z, Cohen RE, Argon AS. Evolution of the crystalline texture of high-density polyethylene during uniaxial compression. Macromolecules 1992;25:4692–704.
[17] Takahashi Y, Puppulin L, Zhu W, Pezzotti G. Raman tensor analysis of ultra-high molecular weight polyethylene and its application to study retrieved hip joint components. Acta Biomater 2009;20(12):1809–22.
[18] Van Gurp M. The use of rotation matrices in the mathematical description of molecular orientations in polymers. Colloid Polym Sci 1995;273:607–25.
[19] Roe RJ. Description of crystallite orientation in polycrystalline materials. III. General solution to pole figure inversion. J Appl Phys 1965;36(6): 2024–31.
[20] Liu T, Kumar S. Quantitative characterization of SWNT orientation by polarized Raman spectroscopy. Chem Phys Lett 2003;378:257–62.
[21] Pezzotti G, Kumakura T, Yamada K, Tateiwa T, Puppulin L, Zhu W, et al. Confocal Raman spectroscopic analysis of cross-linked ultra-high molecular weight polyethylene for application in artificial hip joints. J Biomed Opt 2007;12(1):014011-1–14.
[22] McKellop HA, Shen FW, Yu YJ, Lu B, Salovey R. Effect of sterilization method on the wear rate of UHMWPE acetabular cups in a hip simulator. In: Transactions of the 43rd annual meeting of the Orthopedic Research Society. San Francisco, CA: ORS (Orthopedic Research Society). 1997. p. 94–9.
[23] Premnath V, Harris WH, Jasty M, Merrill EW. Gamma sterilization of UHMWPE articular implants: an analysis of the oxidation problem. Biomaterials 1996;17(18):1741–53.
[24] Tabb DL, Sevcik JJ, Koenig JL. FTIR study of the effects of irradiation on polyethylene. J Polym Sci Polym Phys Ed 1976;13:815–24.
[25] Kumakura T, Puppulin L, Yamamoto K, Takahashi Y, Pezzotti G. In-depth oxidation and strain profiles in UHMWPE acetabular cups non-destructively studied by confocal Raman microprobe spectroscopy. J Biomater Sci Polym Ed 2009;20(12):1809–22.
[26] Geil PH. Polymer single crystals. New York: Wiley Interscience; 1963.
[27] Lin L, Argon AS. Review structure and plastic deformation of polyethylene. J Mater Sci 1994;29:294–323.

[28] Mutter R, Stille W, Strobl GR. Transition regions and surface melting in partially crystalline polyethylene: a Raman spectroscopic study. J Polym Sci B Polym Phys 1993;31:99–105.
[29] Turrell G. In: Gardiner DJ, Graves PR, editors. Raman sampling: practical Raman spectroscopy. Berlin: Springer; 1989. p. 13.
[30] Amer MS, Maguire J, Cai L, Biggers R, Busbee J, LeClair SR. Local grain orientation and strain in polycrystalline $YBa_2Cu_3O_{7-\delta}$ superconductor thin films measured by Raman spectroscopy. J Appl Phys 2001;89(12):8030–4.
[31] Porto SP, Krishnan RS. Raman effect of corundum. J Chem Phys 1967;47:1009–12.
[32] Loudon R. The Raman effect in crystals. Adv Phys 1964;13:423–82.
[33] Puppulin L, Takahashi Y, Zhu W, Pezzotti G. Raman polarization analysis of highly crystalline polyethylene fiber. J Raman Spectrosc 2010. doi: 10.1002/jrs.2725.
[34] Pigeon M, Prud'homme RE, Pézolet M. Characterization of molecular orientation in polyethylene by Raman spectroscopy. Macromolecules 1991;24:5687–94.
[35] Citra MJ, Chase DB, Ikeda RM, Gardner KH. Molecular orientation of high-density polyethylene fibers characterized by polarized Raman spectroscopy. Macromolecules 1995;28:4007–12.
[36] Nikolaeva GY, Semenova LE, Prokhorov KA, Gordeyev SA. Quantitative characterization of macromolecules orientation in polymers by micro Raman spectroscopy. Laser Phys 1997;7(2):403–15.
[37] Pérez R, Banda S, Ounaies Z. Determination of the orientation distribution function in aligned single wall nanotube polymer nanocomposites by polarized Raman spectroscopy. J Appl Phys 2008;103:074302.
[38] Jaynes ET. Information theory and statistical mechanics. Phys Rev 1957;106:620–30.
[39] Galeski A, Bartczak Z, Argon AS, Cohen RE. Morphological alterations during texture-producing plastic plane strain compression of high-density polyethylene. Macromolecules 1992;25:5705–18.
[40] Bartczak Z, Argon AS, Cohen RE. Deformation mechanisms and plastic resistance in single-crystal-textured high-density polyethylene. Macromolecules 1992;25:5036–53.
[41] Bartczak Z. Effect of chain entanglements on plastic deformation behavior of ultra-high molecular weight polyethylene. J Polymer Sci B Polymer Phys 2010;48(3):276–85.
[42] Boontongkong Y, Cohen RE, Spector M, Bellare A. Orientation of plane strain-compressed ultra-high-molecular-weight polyethylene. Polymer 1998;39(25):6391–400.
[43] Atkinson JR, Dowling JM, Cicek RZ. Materials for internal prostheses: the present position and possible future developments. Biomaterials 1980;1(2):89–96.
[44] Glyn-Jones S, McLardy-Smith P, Gill HS, Murray DW. The creep and wear of highly cross-linked polyethylene: a three-year randomized, controlled trial using radiostereometric analysis. J Bone Joint Surg Br 2008;90(5):556–61.
[45] Edidin AA, Herr MP, Villarraga ML, Muth J, Yau SS, Kurtz SM. Accelerated ageing studies of UHMWPE. I. Effect of resin, processing, an radiation environment on resistance to mechanical degradation. J Biomed Mater Res 2002;61(2):312–22.
[46] Muratoglu OK, O'Connor DO, Bragdon CR, Delaney J, Jasty M, Harris WH, et al. Gradient crosslinking of UHMWPE using irradiation in molten state for total joint arthroplasty. Biomaterials 2002;23:717–24.
[47] Muratoglu OK, Bragdon CR, O'Connor DO, Jasty M, Harris WH, Gul R, et al. Unified wear model for highly crosslinked ultra-high molecular weight polyethylenes (UHMWPE). Biomaterials 1999;20:1463–70.